Dalton Transactions

Cite this: *Dalton Trans.*, 2012, **41**, 10465

www.rsc.org/dalton

PAPER

Green synthesis of Au nanoparticles immobilized on halloysite nanotubes for surface-enhanced Raman scattering substrates†

Han Zhu,[a] MingLiang Du,*[a,b] MeiLing Zou,[a] CongSheng Xu[a] and YaQin Fu[a,b]

Received 8th May 2012, Accepted 11th June 2012
DOI: 10.1039/c2dt30998j

A facile and green route was introduced to synthesize Au nanoparticles immobilized on halloysite nanotubes (AuNPs/HNTs) used for surface-enhanced Raman scattering substrates. The naturally occurring HNTs were firstly functionalized with a large amount of $–NH_2$ groups by *N*-(β-aminoethyl)-γ-aminopropyl trimethoxysilane (AEAPTES), which possesses one lone electron pair and will "anchor" Au ions to form a chelate complex. Then, with the addition of tea polyphenols (TP), the Au ions were reduced on the surface of the previously formed Au–NH_2 chelate complex to form AuNPs. Transmission electron microscopy (TEM) and field emission scanning electron microscopy (FE-SEM) observations indicate that a large amount of AuNPs were synthesized on HNTs. The AuNPs are irregularly spherical and densely dispersed on HNTs and the diameter of the nanoparticles varies from 20 to 40 nm. The interactions between AuNPs and $–NH_2$ groups were verified by X-ray photoelectron spectroscopy (XPS) and the results showed that the functional groups can "anchor" AuNPs through the chelating effect. The as-prepared AuNPs/HNTs nanomaterials with several nanometers gaps among nanoparticles were used as a unique surface-enhanced Raman scattering substrate, which possessed strong and distinctive Raman signals for R6G, indicating the remarkable enhancement effect of the AuNPs/HNTs.

1. Introduction

The current exciting cutting edge research in the field of nanotubular materials, such as carbon nanotubes (CNTs) and boron nitride nanotubes (BNNTs), has recently been attracting interest.[1–3] Compared with the above mentioned nanotubes, halloysite nanotubes (HNTs) are readily obtainable, much cheaper and possess a special structure and large reserves in many countries, such as China, New Zealand, Australia, *etc.*[4–7] A mass of researchers have studied the applications of HNTs, such as in catalysis carriers, nanoreactors, entrapment systems for loading, dye or heavy metal adsorbents, storage and controlled release of drugs, anticorrosion agents, biocides and reinforcement of polymers.[4,6–10] HNTs ($Al_2Si_2O_5(OH)_4 \times nH_2O$) possess a hollow tubular structure with an approximately 15 nm lumen, 50 nm external diameter and length of 1000–200 nm. It is a two-layered (1 : 1) aluminosilicate chemically similar to kaolin, with aluminol (Al–OH) groups in the internal surface and Si–OH groups on the external surface, which are potential anchoring sites for nanoparticles.[9,10] Recently, HNTs used as a substrate for the organization of noble metal nanoparticles excitingly attract interest for many potential applications such as catalysis for CO_x-free hydrogen, Cr(VI) removal and photocatalytic degradation of CO_2, owing to their unique optical, electronic, imaging, magnetic and catalytic properties.[5,9,11–14] Meanwhile, gold nanostructures have been the focus of intense research owing to their fascinating optical, electronic, and chemical properties and promising applications in catalysis, nanoelectronics, biomedicine and surface-enhanced Raman scattering (SERS).[14–20] SERS is one of the most powerful probing tools for biochemical applications and trace detection of organic chemicals because it enables ultrasensitive, low-cost and real-time detection.[21–24] A large amount of research works have demonstrated that the giant signal amplification in SERS arises from the electromagnetic enhancement at so-called 'hot spots', which may be in either interstitial voids of metal nanoparticles or metal structures with intersections, bifurcations and high radii of curvature. Although SERS effects can be achieved simply by exploiting the electromagnetic resonance properties of roughened surfaces or nanoparticles of Au or Ag, the fabrication of reliable SERS substrates with uniformly high enhancement factors remains the focus of much research.

There are various methods for the synthesis of AuNPs, however, most are either complex or time-consuming, or require strict synthetic conditions.[24–26] The previous widely employed reducing agents for synthesizing AuNPs, such as sodium borohydride, *N*,*N*-dimethylformamide (DMF) and hydrazine, *etc.*, are highly active or have potential environmental risk for wide applications. There are three main criteria for a "green" synthesis of nanoparticles: an environmentally compatible solvent system, an

[a]*Department of Materials Engineering, College of Materials and Textile, Zhejiang Sci-Tech University, Hangzhou 310018, P.R. China*
[b]*Key Laboratory of Advanced Textile Materials and Manufacturing Technology, Zhejiang Sci-Tech University, Ministry of Education, Hangzhou 310018, P. R. China. E-mail: du@zstu.edu.cn; Tel: +86-571-86843255*

†Electronic supplementary information (ESI) available. See DOI: 10.1039/c2dt30998j

eco-friendly reducing agent and a non-hazardous capping agent for stabilizing the nanoparticles.[27–31] Nowadays, there has been an increased emphasis on the greener production of environmentally benign and renewable materials as the respective reducing and stabilizing agents. In our previous work,[32] we have firstly introduced the green natural compounds, tea polyphenols (TP) both serving as a reducer and stabilizer, to synthesize AuNPs successfully. The green TP are groups of water-soluble polyphenol compounds richly deposited in plants, belonging to the flavonoid family, and mainly include epicatechin (EC), epicatechin gallate (ECG), epigallocatechin (EGC) and epigallocatechin gallate (EGCG), in which the EGCG makes up about 46% of the total TP.[30–35] Wang *et al.* have successfully synthesized TiO_2 nanoparticles/HNTs nanostructure *via* depositing the TiO_2 nanoparticles onto HNTs and Zhu *et al.* have reported the preparation of HNTs-supported Ru nanoparticles.[5,9] However, there are no reports about the application of AuNPs immobilized on HNTs for SERS substrates. Meanwhile, it remains challenging to obtain a cheap, reliable, stable and uniform SERS signal spanning a wide dynamical range.

In the present investigation, due to the advantages of HNTs, such as the special nanotubular structure, high specific area and high absorption ability, we immobilized AuNPs onto the surface of HNTs to create more 'hot spots' for the enhancement of SERS signals. *N*-β-Aminoethyl-γ-aminopropyl trimethoxysilane (AEAPTES) is composed of a large number of primary and secondary amino groups in a molecule. As reported, the amino groups possess lone electron pairs, which can catch the noble metal ions to form a chelate complex through the chelating effect and exhibit good stability for immobilizing nanoparticles onto HNTs.[11,36] In our present study, we introduce a two-step method to synthesize AuNPs immobilized on HNTs (AuNPs/HNTs). Firstly, HNTs were functionalized by grafting AEAPTES onto HNTs and then, we used TP as a reducing agent and stabilizer to synthesize AuNPs/HNTs through an *in situ* approach. A series of characterizations were made to test and confirm the present investigations. The as-prepared AuNPs/HNTs nanomaterials have been used as a surface-enhanced Raman scattering substrate, which possessed strong and distinctive Raman signals for R6G, indicating the remarkable enhancement effect.

2. Experiment section

2.1 Materials

The halloysite nanotubes (HNTs) were collected from Hubei Province, China. The Brunauer–Emmett–Teller (BET) specific surface area was determined as 50.45 $m^2\ g^{-1}$. Chloroautic acid ($HAuCl_4{\cdot}3H_2O$, 99.9%) was acquired from Shanghai Civi Chemical Technology Co., Ltd, China. Tea polyphenols (TP) were purchased from Xuancheng BaiCao Plant Industry and Trade Co., Ltd, China. *N*-(β-Aminoethyl)-γ-aminopropyl trimethoxysilane (AEAPTES, $NH_2CH_2CH_2NHCH_2CH_2CH_2$ Si-$(OCH_3)_3$) was purchased from Sinopharm Chemical Reagent Co., Ltd, China.

2.2 Functionalization of HNTs using AEAPTES

The HNTs were firstly purified *via* a repeated washing/centrifugation process and then dried at 80 °C in a vacuum oven for 12 hours. 5 g AEAPTES was dissolved in 95 g 95% ethanol and then an appropriate amount of acetic acid was drop into the mixture to make the pH reach a constant value of about 4. The mixture was stirred vigorously at room temperature for 1.5 hours. Next, 5 g HNTs were added to the as-prepared solution and the mixture was kept under refluxing conditions for 6 hours at 80 °C. The functionalized HNTs were purified *via* a repeated washing/centrifugation process with ethanol to remove ungrafted AEAPTES and possible products of hydrolysis. Then, the functionalized HNTs were dried for 12 hours in an oven under vacuum at 80 °C and used for further experiments.

2.3 Synthesis of the Au nanoparticles immobilized on HNTs

$HAuCl_4{\cdot}3H_2O$ was dissolved in deionized water to get a 10.0 mmol L^{-1} Au^{3+} solution. 15 mL Au^{3+} solution was dropped in 30 mL HNTs solution (dissolved 0.5 g functionalized HNTs in 30 mL deionized water) and then the mixture was heated to 45 °C and stirred vigorously for 1 h. At last, 0.034 g TP dissolved in 5 mL deionized water were added to the mixture. After 15 minutes, the as-prepared powder was purified *via* repeated washing/centrifugation process with ethanol and then dried in vacuum oven at 80 °C and used for further experiments and characterizations.

2.4 SERS measurements

For SERS studies, a Thermo Scientific Nicolet NXR Fourier Transform Raman was used to carry out the SERS measurement and the as-synthesized AuNPs/HNTs were used as SERS substrates. R6G has been extensively studied and well-characterized by SERS, and in this study it was chosen as a model analyte to investigate the performance of the as-prepared AuNPs/HNTs substrate for SERS detection. 0.005 g HNTs and AuNPs/HNTs were dipped in 1 mL R6G (from 10^{-3} M to 10^{-6} M) aqueous solution for 30 min and then were dropped onto the Si substrate and dried under an infrared lamp. 1 mL AuNPs in aqueous solution were mixed with 1 mL R6G solution and then dropped in NMR tube for SERS measurements, which was used as a control.

2.5 Characterization

2.5.1 X-ray diffraction (XRD). The crystal structure of HNTs and AuNPs/HNTs were characterized with a SIEMENS Diffraktometer D5000 X-ray diffractometer using a Cu Kα radiation source at 35 kV, with a scan rate of 0.02° $2\theta\ s^{-1}$ in the 2θ range of 10–80°.

2.5.2 Fourier transform infrared spectroscopy (FTIR). The pure HNTs powder and the as-synthesized functionalized HNTs powder were spread on KBr pellets individually and then dried under an infrared lamp. The FTIR analysis was conducted by a Nicolet 5700 FTIR spectrometer.

2.5.3 Transmission electron microscopy (TEM). The HNTs and the as-synthesized AuNPs/HNTs were dissolved in diluted water solution and respectively dropped on the ultra-thin carbon-coated copper grid and dried under an infrared lamp for

5 minutes. The images were acquired using a JSM-2100 transmission electron microscopy (TEM, JEOL, Japan) at an accelerating voltage of 200 kV.

2.5.4 Scanning electron microscopy (SEM). The HNTs powders were spread on the conducting adhesive and the images were acquired using a LEO 1530 VP SEM machine.

2.5.5 Field emission scanning electron microscopy (FE-SEM). The morphology of the AuNPs/HNTs powder was observed by a ULTRA-55 field-emission scanning electron microscope (FE-SEM, JEOL, Japan).

2.5.6 X-ray photoelectron spectroscopy (XPS). X-ray photoelectron spectra of pure HNTs powder and AuNPs/HNTs powder were recorded by using an X-ray photoelectron spectrometer (Kratos Axis Ultra DLD) with an aluminum (mono) Kα source (1486.6 eV). The aluminum Kα source was operated at 15 kV and 10 mA. For all of the samples, in order to obtain more information about the chelating effect, a high-resolution survey (pass energy = 48 eV) was performed at spectral regions relating to gold and nitrogen.

2.5.7 Fourier Transform Raman (FT-Raman). A Thermo Scientific Nicolet NXR Fourier Transform Raman spectrometer was used to carry out the SERS measurement. An argon ion laser of 1064 nm at a spectral resolution of 4 cm^{-1} and a spot size of 1 μm was used for excitation. The laser power on the specimens was measured at 0.3 mW. The recorded spectra were raw data without any background subtraction or processing.

2.5.8 Ultraviolet-visible spectroscopy (UV-Vis). The spectra of pure HNTs and as-prepared AuNPs/HNTs powder were collected by a Lambda 900 UV-Vis spectrophotometer (Perkin Elmer, USA). All of the spectra were collected over a wavelength range of 200–800 nm.

3 Results and discussion

3.1 Morphology of HNTs and functionalization of HNTs using AEAPTES

The structure and morphology of the HNTs were observed by TEM and SEM. Fig. 1a displays the TEM image of naturally occurring HNTs and the predominant form is a hollow tubular structure in the submicrometer range. The size of the inner and outer diameters of the halloysite tubules are about 15–20 and 40–50 nm, respectively, depending on the deposit condition. The lumen length of the natural HNTs ranging 500–2000 nm is shown in Fig. 1b, indicating the polydispersity of HNTs in length.

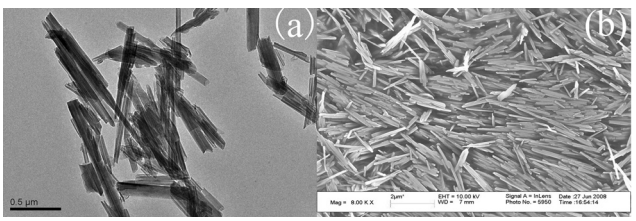

Fig. 1 The TEM (a) and SEM (b) images of HNTs.

FTIR analysis was conducted to investigate the chemical changes during the reaction process and testify the grafted AEAPTES onto HNTs. The photographs of pure HNTs powder, functionalized HNTs powder and AuNPs/HNTs powder are shown in Fig. 1S (see ESI†). Fig. 2 shows the FTIR spectra of pure HNTs powders (curve a) and the functionalized HNTs powders (curve b). The characteristic peaks of HNTs that occurred at 3698 cm^{-1}, 3623 cm^{-1} and 1634 cm^{-1} are attributed to O–H stretching of inner-surface hydroxyl groups, O–H stretching of inner hydroxyl groups and deformation of water, respectively. These absorption peaks have no change after modification, suggesting that the basic structure of HNTs and functionalized HNTs remain constant.[5,7,9–11] However, several absorption peaks at 2927 cm^{-1}, 2860 cm^{-1} and 1381 cm^{-1} are newly emerged, which are attributed to C–H asymmetric and symmetric stretching vibrations of AEAPTES, respectively.[11] The band at 3452 cm^{-1} is assigned to the stretching vibration of N–H. The intensity of the peaks observed at 1109 cm^{-1} and 1034 cm^{-1} ascribed to in-plane stretching of Si–O increase and become relatively narrow, which can also imply the existence of AEAPTES grafted on the HNTs.[37–39] The above results can demonstrate that AEAPTES, the sole source for C–H and N–H, has successfully been grafted onto the HNTs.

To prove that the AEAPTES were chemically bonded onto HNTs, the XPS spectra of the pure HNTs powder and functionalized HNTs powder are investigated and the spectra of O 1s are presented in Fig. 3. As observed in Fig. 3a, the intense characteristic peak that emerged at 531.7 eV corresponds well with O 1s of pure HNTs powder binding energy. After the functionalization of HNTs by AEAPTES, the binding energy of O 1s is increased to 532.5 eV, indicating that the AEAPTES has successfully grafted on the HNTs. The chemical changes during the reaction process are shown in Fig. 2S (see ESI†).

3.2 Synthesis of the AuNPs immobilized on HNTs

A facile and green approach was introduced to synthesize AuNPs/HNTs using tea polyphenols (TP) as the reductant. The

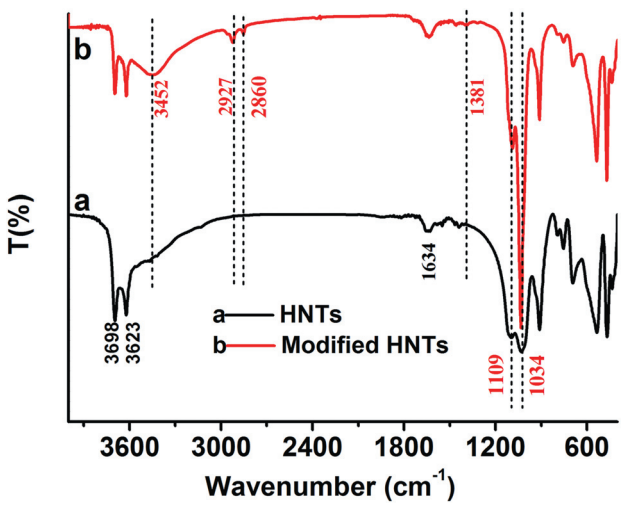

Fig. 2 FTIR spectra of HNTs (curve a) and functionalized HNTs using AEAPTES (curve b).

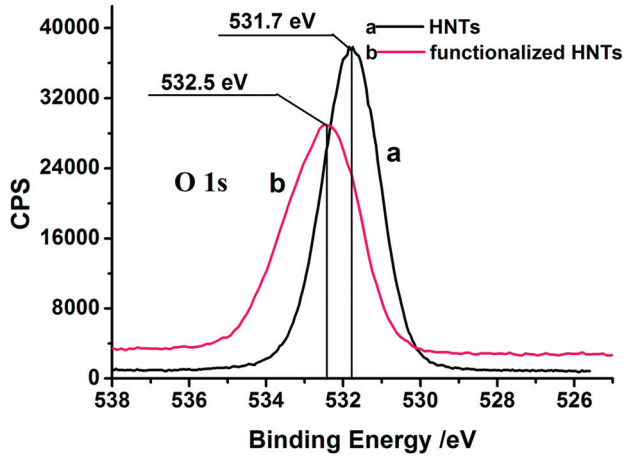

Fig. 3 The XPS spectra of the HNTs before and after surface functionalization by AEAPTES: (a) O 1s of pure HNTs powder (b) O 1s of functionalized HNTs by AEAPTES.

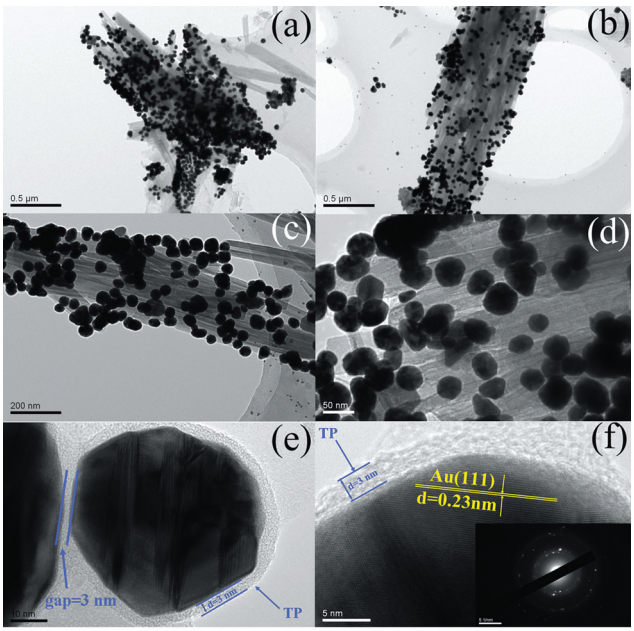

Fig. 4 (a–e) TEM images of AuNPs/HNTs; (f) a HRTEM image of the AuNP and the insert is the corresponding selected area electron diffraction pattern.

morphology and structure of the as-synthesized AuNPs/HNTs are shown in Fig. 4.

As shown in Fig. 4a and b, a large amount of AuNPs were immobilized on the HNTs. The AuNPs are irregularly spherical and densely dispersed on the HNTs and the diameter of the nanoparticles varies from 20 to 40 nm, which can be seen in Fig. 4c and d. Fig. 4e shows that the AuNPs are surrounded by a layer of TP and the thickness of the layer is about 3 nm.

Due to the stabilization of TP,[31,32] the AuNPs separated well and nearly no aggregations are observed. The high resolution TEM image (Fig. 4f) shows that the lattice fringes are visible with a spacing of about 0.23 nm, which corresponds to the lattice spacing of the (111) planes of Au.[30–32] As shown in Fig. 4f, the electron diffraction pattern of the corresponding

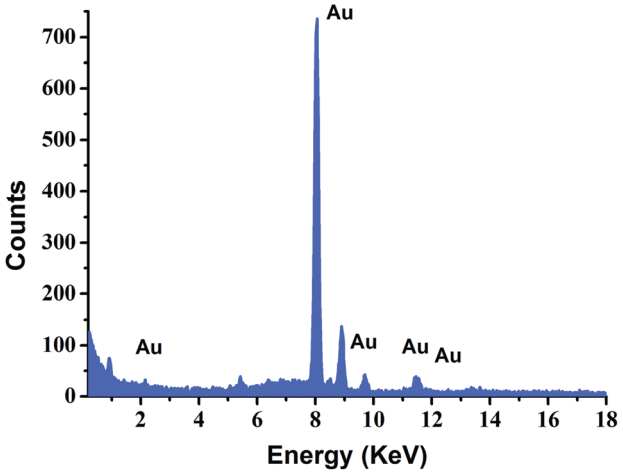

Fig. 5 The EDX spectrum of the AuNPs immobilized on HNTs.

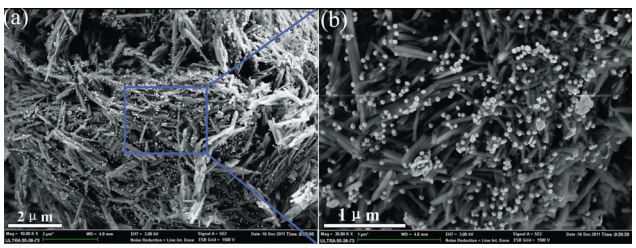

Fig. 6 (a, b) FE-SEM images of the AuNPs/HNTs.

selected area of AuNPs indicate the polycrystallinity of AuNPs and the diffuse ring confirm the existence of TP.

The EDX spectrum of the AuNPs immobilized on HNTs is shown in Fig. 5. The EDX spectrum only exhibits the characteristic peaks of Au, suggesting that the obtained product is composed of pure Au and confirming the existence of AuNPs immobilized on HNTs. Besides, the UV-Vis spectra of HNTs and AuNPs also indicate that the surface plasmon resonance absorption peak of AuNPs is 537 nm, as shown in Fig. 3S (see ESI†).

From the FE-SEM images shown in Fig. 6, quantities of well-dispersed AuNPs were immobilized on the surface of HNTs, which is in accordance with the TEM results (Fig. 4). Notably, the AuNPs were irregularly dispersed on the surface of the HNTs, which indicates that the AuNPs were synthesized and immobilized on the surface of HNTs and it was believed that this will display a promising and potential prospect for SERS detection.

To further confirm the presence of the AuNPs, the HNTs and AuNPs/HNTs powder were characterized by XRD and the diffraction patterns of HNTs before and after the immobilization of AuNPs are shown in Fig. 7. According to the literature,[5,9] all of the observed peaks mainly can be indexed to the characteristic peaks of HNTs, as shown in curve A. Some of the characteristic peaks reduced after the immobilization of AuNPs. However, four new peaks emerged, a new stronger peak at $2\theta = 38.1^{\circ}$ and three relatively weak peaks at $2\theta = 44.4^{\circ}$, 64.6° and 77.6°, which exactly match with the reference values for the Au (111), Au (200), Au (200) and Au (311) lattice planes, respectively.[20,31,37] All of the peaks are characteristic of face-centered cubic (fcc)

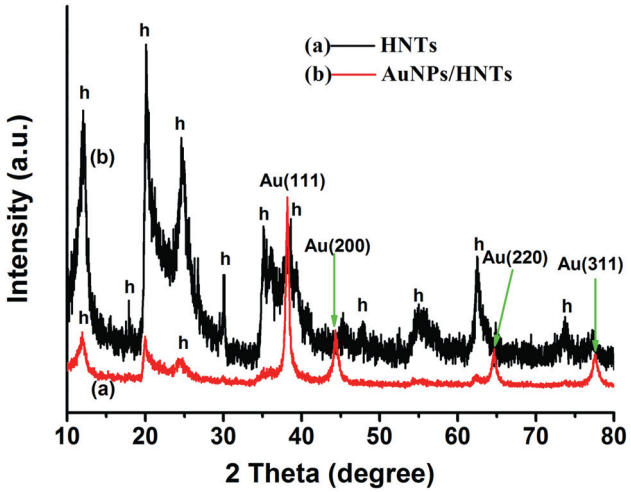

Fig. 7 The XRD patterns of HNTs powder (curve a) and AuNPs/HNTs powder (curve b). (h: HNTs).

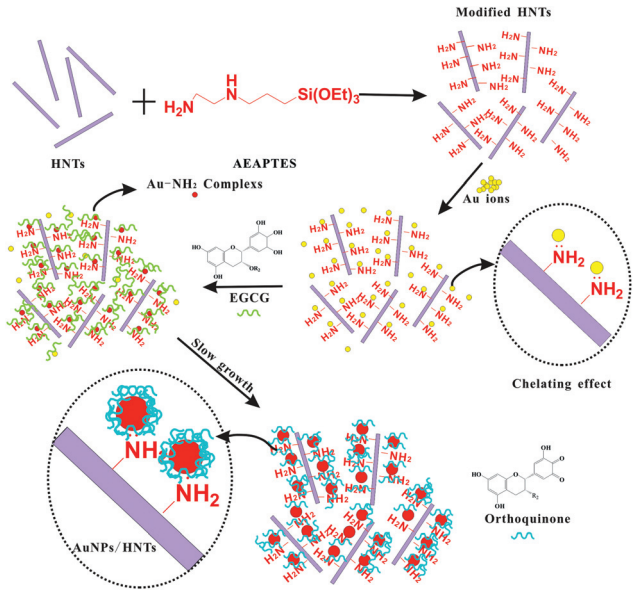

Scheme 1 A schematic illustration of the synthesis of the AuNPs immobilized on HNTs.

gold (JCPDS-4748).[31,32] From the above results, it can be further confirmed that the AuNPs/HNTs were successfully synthesized.

The present process is schematically illustrated in Scheme 1. Firstly, the surface of HNTs are functionalized with $–NH_2$ by AEAPTES. As is well-known, the functionalized HNTs possess a large amount of $–NH_2$ groups, which have one lone electron pair and can form a chelating complex with Au ions.[11,30,32] Due to the chelating effects between Au ions and $–NH_2$ groups, most of the Au ions were "anchored" by the $–NH_2$ groups, resulting in the formation of Au–NH_2 complexes. Then, with the addition of TP, the previously formed Au–NH_2 complexes can also chelate with the phenolic hydroxyls of TP and, meanwhile, the Au ions were reduced by TP. Consequently, besides the chelating effects, the TP can also used as a stabilizer to protect the AuNPs from aggregation. As the reaction proceeded, other Au ions were further diffused to the Au–NH_2 complexes region and reduced on the surface of Au–NH_2 complexes by TP with the oxidation of the phenolic hydroxyls to orthoquinone.[30–33] As a consequence, the synthesized AuNPs were wrapped with a layer of TP, which can be observed in Fig. 4e and f. The chelating effect between Au ions and $–NH_2$ groups will be testified later.

The chelating effects of AuNPs with $–NH_2$ groups were testified by XPS analysis. The chemical state of the AuNPs immobilized on the functionalized HNTs is presented in Fig. 8. As observed in Fig. 8a, the intense doublets that emerged at 88.3 eV and 84.6 eV correspond well with Au $4f_7$ and Au $4f_5$ binding energies, respectively. Compared with zero valent Au^0 (87.7 eV and 84.0 eV), the changes of the binding energy indicate the interaction between AuNPs and $–NH_2$ groups.[31,32] Negishi *et al.* have also pointed out that the Au 4f peaks occurring at relatively higher binding energy can be attributed to the surface Au atoms of AuNPs bonded to the surface surrounding the stabilizer or passive molecules, suggesting that a substantial electron donation from AuNPs to stabilizer molecules is present.[40] Fig. 8b shows the nitrogen 1s XPS spectrum of the functionalized HNTs; two peaks occurred at 399.5 eV and 401.6 eV, standing for two chemical states of nitrogen in HNTs. However, the binding energies of nitrogen 1s observed in Fig. 8c shift to 400.2 eV and 402.1 eV, demonstrating the strong interaction between AuNPs and $–NH_2$ groups. In conclusion, all of the above results can confirm the chelating effects between the AuNPs and $–NH_2$ groups and the functional groups can "anchor" AuNPs through the chelating effect, which shows an exciting prospect for immobilization of AuNPs.

SERS has become a powerful technique to detect chemical and biological molecules toward single-molecule detection sensitivity. AuNPs have been widely used as the SERS source due to their intriguing and strong SERS activity.[41–44] As reported, AuNPs with different morphologies, such as gold nanoparticles, nanorods and nanoflowers have been used as the SERS substrate. Here, AuNPs immobilized on HNTs were used as SERS substrates to detect Rhodamine 6G (R6G), a typical model analyte for SERS performance evaluation.[42–45]

As exemplified by Fig. 9, curve a displays very weak Raman signals for a 10^{-3} M R6G aqueous solution enhanced by AuNPs and there is nearly no enhancement effect of R6G on the HNTs without AuNPs (curve b). Notably, the AuNPs/HNTs SERS substrates (curve c) show strong and distinctive Raman signals for R6G, indicating the remarkable enhancement effect on the AuNPs immobilized on HNTs. Three different concentrations of R6G aqueous solution (from 10^{-3} M to 10^{-6} M) were applied in the SERS test using AuNPs/HNTs as the SERS substrates and the results are shown in Fig. 10. Prominent Raman bands of R6G at 1650, 1505, 1362, 1305 and 1181 cm^{-1} are observed in Fig. 9 and 10. The peak at 1180 cm^{-1} is associated with C–C in-plane bend modes, and the signals between 1306 and 1650 cm^{-1} are due to aromatic C–C stretching vibrations.[41,46] When the amount of R6G on the AuNPs/HNTs substrate was reduced to 10^{-6} M (1 mL aqueous solution), some peaks of R6G molecules were still observed, as shown in curve c, which contains the same characteristic Raman peaks of R6G in common with curves a and b. These indicated that the AuNPs/HNTs substrate possessed a relativly high surface enhancement efficiency and showed a promising prospect for application as SERS substrates.

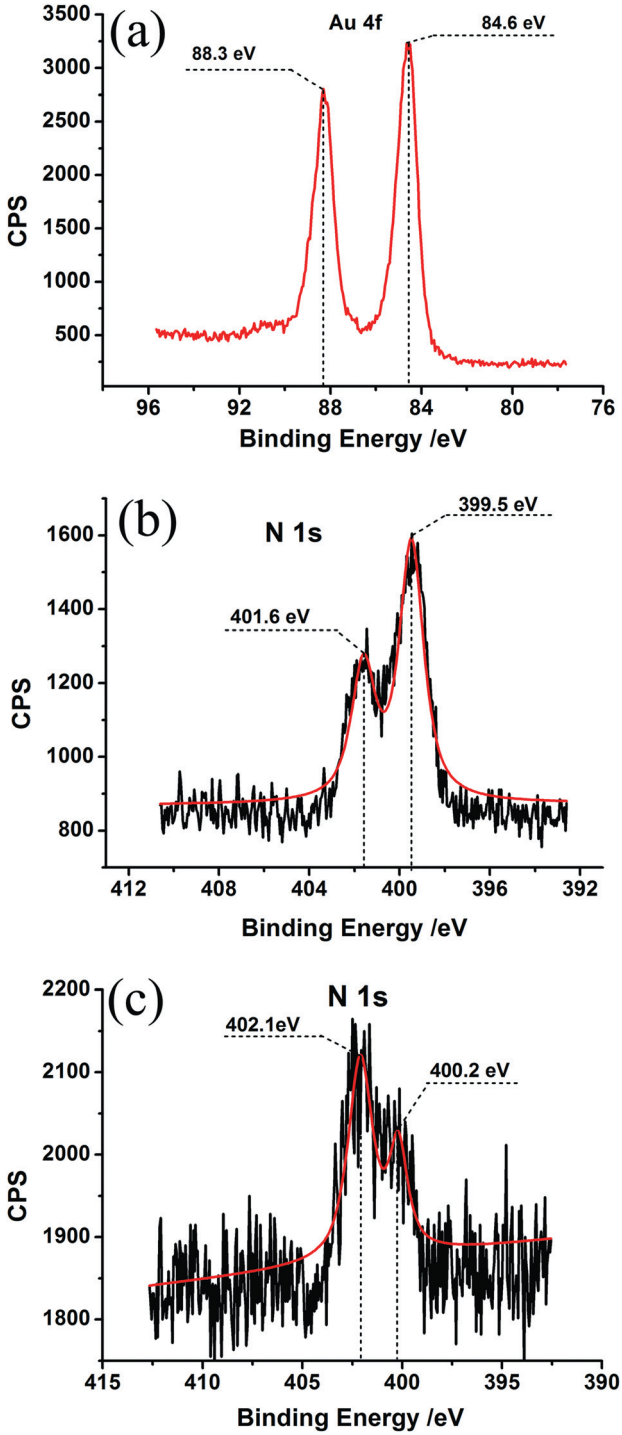

Fig. 8 XPS spectra of the functionalized HNTs before and after surface functionalization with AuNPs (a) Au 4f of AuNPs/HNTs; (b) N 1s of functionalized HNTs; (c) N 1s of AuNPs/HNTs.

According to the electromagnetic theory of SERS, the size, shape and proximity of nanostructures all affect the frequency and magnitude of the localized surface plasmons, *i.e.*, the degree of Raman enhancement.[43] The widely accepted SERS enhancement theory is electromagnetic enhancement at so-called 'hot spots' and several theoretical groups have investigated field enhancement for SERS from metal nanoparticle arrays. Garcia-Vidal and Pendry reported that very localized plasmon modes,[43]

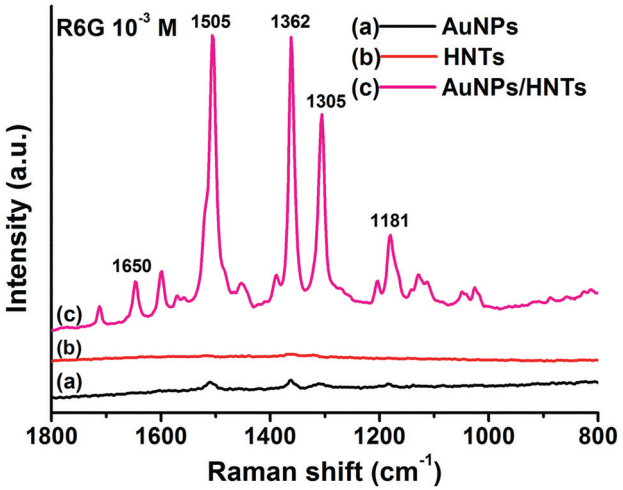

Fig. 9 SERS spectra of 1 mL 10^{-3} M R6G collected on (a) AuNPs in aqueous solution, (b) pure HNTs powder, (c) AuNPs/HNTs powder.

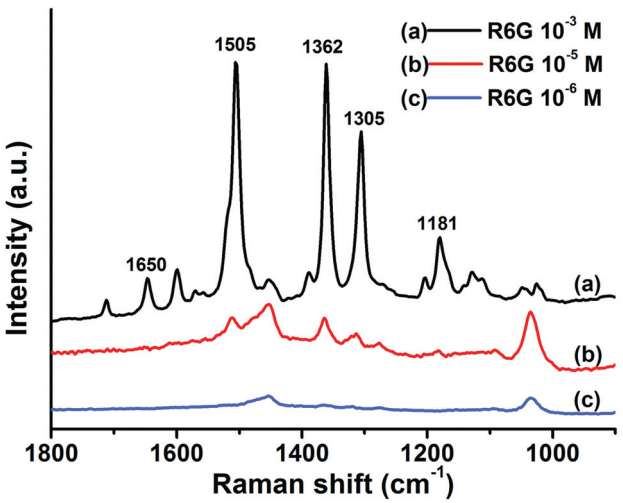

Fig. 10 SERS spectra obtained from AuNPs/HNTs with 1 mL of R6G solution of different concentrations: (a) 10^{-3} M R6G, (b) 10^{-5} M R6G and (c) 10^{-6} M R6G.

created by strong electromagnetic coupling between two adjacent metallic objects, dominate the SERS response in an array of nanostructures. In our present investigation, a large amount of AuNPs were densely dispersed on HNTs and the gaps among nanoparticles were about several nanometers, which can be seen in Fig. 4. According to the literatures,[44,47–49] the interparticle-coupling-induced enhancement was attributed to the broadening of the plasmon resonance peak because the probability of the resonance covering both the excitation wavelength and the Raman peak increases with its width. Wang *et al.* have studied highly Raman-enhancing substrates based on silver nanoparticle arrays with tunable sub-10 nm gaps and pointed out the great SERS enhancement effect on a substrate with precisely controlled 'hot junctions' in the sub-10 nm region, which also confirmed the theoretical prediction of interparticle-coupling-induced Raman enhancement.[44] To investigate the localized surface plasmon resonance effect in the AuNPs/HNTs substrate, the UV-Vis spectra of AuNPs/HNTs was recorded by UV-Vis spectroscopy, as shown in Fig. 3S (see ESI†). Generally, the

peak shape and position of SPR in UV-Vis spectra are dependent on the size, shape, arrangement (*e.g.*, density and interparticle spacing) and the surrounding dielectric constant of AuNPs.[32,41,50] In our present work, the AuNPs immobilized on HNTs with high density and close gaps between two nanoparticles, and the dipoles induced by plasmon resonance would couple and transmit on the whole substrate. Consequently, the plasmon resonance absorption of our substrate is broad and strong, which is evidence for the high enhancement effect of the AuNPs/HNTs substrate. Consequently, the roughness of AuNPs/HNTs and the characteristics of AuNPs, *i.e.*, size, low gaps, separation and high density, immobilized on HNTs may provide an optimum environment for the enhancement in Raman signals. The above results indicated that the AuNPs/HNTs substrate possessed a relativly high surface enhancement efficiency and showed a promising prospect for application as SERS substrates.

4. Conclusion

In the present investigation, a facile and green route was proposed to synthesise AuNPs/HNTs used for surface-enhanced Raman scattering substrates. HNTs were firstly functionalized with $-NH_2$ by *N*-(β-aminoethyl)-γ-aminopropyl trimethoxysilane (AEAPTES), which "anchors" Au ions to form a chelate complex. Then, with the addition of TP, the Au–NH_2 complexes can also chelate with the phenolic hydroxyls of TP and, meanwhile, the Au ions were reduced by TP. Besides the chelating effects, the TP can also be used as stabilizer to protect the AuNPs from aggregation. TEM, SEM and FE-SEM observations indicate that a large amount of Au nanoparticles were immobilized on HNTs. The AuNPs are irregularly spherical and densely dispersed on HNTs and the diameter of the nanoparticles varies from 20 to 40 nm. The chelating interactions between AuNPs and $-NH_2$ groups were verified by XPS spectra. The as-prepared AuNPs/HNTs nanomaterials with several nanometers gaps among nanoparticles were used as a unique surface-enhanced Raman scattering substrate, which possessed strong and distinctive Raman signals for R6G, indicating the remarkable enhancement effect of the AuNPs/HNTs.

Acknowledgements

This work is supported by the project of National Natural Science Foundation of China (NSFC) (Grant number: 50903072), Zhejiang Province Natural Science Foundation (Grant number: Y4100197) and Science Foundation of Zhejiang Sci-Tech University (ZSTU) under No. 0901803-Y.

References

1 P. Serp and E. Castillejos, *ChemCatChem*, 2010, **2**, 41–47.
2 X. L. Pan and X. H. Bao, *Chem. Commun.*, 2008, 6271–6281.
3 S. J. Guo, J. Li, W. Ren, D. Wen, S. J. Dong and E. K. Wang, *Chem. Mater.*, 2009, **21**, 2247–2257.
4 Y. M. Lvov, D. G. Shchukin, H. Mohwald and R. R. Price, *ACS Nano*, 2008, **2**, 814–820.
5 R. J. Wang, G. H. Jiang, Y. W. Ding, Y. Wang, X. K. Sun, X. H. Wang and W. X. Chen, *ACS Appl. Mater. Interfaces*, 2011, **3**, 4154–4158.
6 M. L. Du, B. C. Guo and D. M. Jia, *Polym. Int.*, 2010, **59**, 574–582.
7 M. L. Du, B. C. Guo, M. X. Liu, X. J. Cai and D. M. Jia, *Physica B*, 2010, **405**, 655–662.
8 C. Y. Wan, M. Li, X. Bai and Y. Zhang, *J. Phys. Chem. C*, 2009, **113**, 16238–16246.
9 L. Wang, J. L. Chen, L. Ge, Z. H. Zhu and V. Rudolph, *Energy Fuels*, 2011, **25**, 3408–3416.
10 M. X. Liu, B. C. Guo, M. L. Du, F. Chen and D. M. Jia, *Polymer*, 2009, **50**, 3022–3030.
11 P. Luo, J. S. Zhang, B. Zhang, J. H. Wang, Y. H. Zhao and J. D. Liu, *Ind. Eng. Chem. Res.*, 2011, **50**, 10246–10252.
12 X. Zhang, H. Wang and B. Q. Xu, *J. Phys. Chem. B*, 2005, **109**, 9678–9683.
13 D. Astruc, *Inorg. Chem.*, 2007, **46**, 1884–1894.
14 S. L. Smitha, K. G. Gopchandran, T. R. Ravindran and V. S. Prasad, *Nanotechnology*, 2011, **22**, 265705–265711.
15 Y. Qin, A. L. Pan, L. F. Liu, O. Moutanabbir, R. B. Yang and M. Knez, *ACS Nano*, 2011, **5**, 788–794.
16 R. M. Finch, N. A. Hodge, G. J. Hutchings, A. Meagher, Q. A. Pankhurst, M. R. H. Siddiqui, F. E. Wagner and R. Whyman, *Phys. Chem. Chem. Phys.*, 1999, **1**, 485–489.
17 F. Cardenas-Lizana, S. Gomez-Quero, N. Perret and M. A. Keane, *Catal. Sci. Technol.*, 2011, **1**, 652–661.
18 S. G. Jang, A. Khan, M. D. Dimitriou, B. J. Kim, N. A. Lynd, E. J. Kramer and C. J. Hawker, *Soft Matter*, 2011, **7**, 6255–6263.
19 S. Murru, A. A. Gallo and R. S. Srivastava, *ACS Catal.*, 2011, **1**, 29–31.
20 M. N. Nadagouda, G. Hoag, J. Collins and R. S. Varma, *Cryst. Growth Des.*, 2009, **9**, 4979–4983.
21 Y. Y. Jiang, X. J. Wu, Q. Li, J. J. Li and D. S. Xu, *Nanotechnology*, 2011, **22**, 385601–385607.
22 Y. J. Chen, G. H. Tian, K. Pan, C. G. Tian, J. Zhou, W. Zhou, Z. Y. Ren and H. G. Fu, *Dalton Trans.*, 2012, **41**, 1020–1026.
23 C. H. Lee, L. M. Tian, A. Abbas, R. Kattumenu and S. Singamaneni, *Nanotechnology*, 2011, **22**, 275311–275318.
24 J. Yin, T. Wu, J. B. Song, Q. Zhang, S. Y. Liu, R. Xu and H. W. Duan, *Chem. Mater.*, 2011, **23**, 4756–4764.
25 G. M. Kim, A. Wutzler, H. J. Radusch, G. H. Michler, P. Simon, R. A. Sperling and W. J. Parak, *Chem. Mater.*, 2005, **17**, 4949–4957.
26 M. C. Daniel and D. Astruc, *Chem. Rev.*, 2004, **104**, 293–346.
27 S. J. Guo and E. Wang, *Nano Today*, 2011, **6**, 240–264.
28 M. N. Nadagouda and R. S. Varma, *Green Chem.*, 2008, **10**, 859–862.
29 E. Gonzalez, J. Arbiol and V. F. Puntes, *Science*, 2011, **334**, 1377–1380.
30 W. J. Parak, *Science*, 2011, **334**, 1359–1360.
31 H. Wu, X. Huang, M. M. Gao, X. P. Liao and B. Shi, *Green Chem.*, 2011, **13**, 651–658.
32 H. Zhu, M. L. Du, M. L. Zou, C. S. Xu, N. Li and Y. Q. Fu, *J. Mater. Chem.*, 2012, **22**, 9301–9307.
33 M. C. Moulton, L. K. Braydich-Stolle, M. N. Nadagouda, S. Kunzelman, S. M. Hussain and R. S. Varma, *Nanoscale*, 2010, **2**, 763–770.
34 L. Peng, X. X. Wang, X. G. Shi, C. G. Li, C. G. Ye and X. H. Song, *Food Chem.*, 2011, **129**, 1475–1482.
35 H. Y. Jiang, T. Shii, Y. Matsuo, T. Tanaka, Z. H. Jiang and I. Kouno, *Food Chem.*, 2011, **129**, 830–836.
36 C. Deng, N. Yao, X. Lu, S. X. Qu, B. Feng, J. Weng and X. B. Yang, *J. Mater. Sci.*, 2009, **44**, 4394–4398.
37 I. Gorelikov and N. Matsuura, *Nano Lett.*, 2008, **8**, 369–373.
38 J. M. Pan, H. Yao, L. C. Xu, H. X. Ou, P. W. Huo, X. X. Li and Y. S. Yan, *J. Phys. Chem. C*, 2011, **115**, 5440–5449.
39 G. Ma, X. G. Yue, S. L. Zhang, C. R. Rong, L. F. Wang, G. B. Wang and H. L. Wang, *Polym. Eng. Sci.*, 2011, **51**, 1051–1058.
40 Y. Negishi, K. Nobusada and T. Tsukuda, *J. Am. Chem. Soc.*, 2005, **127**, 5261.
41 M. F. Peng, J. Gao, P. P. Zhang, Y. Li, X. H. Sun and S. T. Lee, *Chem. Mater.*, 2011, **23**, 3296–3301.
42 J. X. Fang, S. Y. Du, S. G. Lebedkin, Z. Y. Li, R. Kruk, M. Kappes and H. Hahn, *Nano Lett.*, 2010, **10**, 5006–5013.
43 H. H. Wang, C. Y. Liu, S. B. Wu, N. W. Liu, C. Y. Peng, T. H. Chan, C. F. Hsu, J. K. Wang and Y. L. Wang, *Adv. Mater.*, 2006, **18**, 491–495.
44 H. Wang and J. N. Halas, *Adv. Mater.*, 2008, **20**, 820–825.
45 D. He, B. Hu, Q. F. Yao, K. Wang and S. H. Yu, *ACS Nano*, 2009, **12**, 3993–4002.
46 P. Hildebrandt and M. J. Stockburger, *Phys. Chem.*, 1984, **88**, 5935–5944.
47 C. F. Tian, *et al.*, *Nanotechnology*, 2012, **23**, 165604–165610.
48 Y. H. Feng, S. X. Xing, J. Xu, H. Wang, J. W. Lim and H. Y. Chen, *Dalton Trans.*, 2010, **39**, 349–351.
49 C. Q. Chen, Y. H. Zheng, Y. Y. Zhan, X. Y. Lin, Q. Zheng and K. M. Wei, *Dalton Trans.*, 2011, **40**, 9566–9570.
50 J. He, P. Zhang, J. L. Gong and Z. H. Nie, *Chem. Commun.*, 2012, DOI: 10.1039/c2cc32070c.